Dissociating Early and Late Error Signals in Perceptual Recognition

Mark E. Wheeler[1], Steven E. Petersen[2], Steven M. Nelson[2], Elisabeth J. Ploran[1], and Katerina Velanova[1]

Abstract

■ Decisions about object identity follow a period in which evidence is gathered and analyzed. Evidence can consist of both task-relevant external stimuli and internally generated goals and expectations. How the various pieces of information are gathered and filtered into meaningful evidence by the nervous system is largely unknown. Although object recognition is often highly efficient and accurate, errors are common. Errors may be related to faulty evidence gathering arising from early misinterpretations of incoming stimulus information. In addition, errors in task performance are known to elicit late corrective performance monitoring mechanisms that can optimize or otherwise adjust future behavior. In this study, we used functional magnetic resonance imaging (fMRI) in an extended trial paradigm of object recognition to study whether we could identify performance-based signal modulations prior to and following the moment of recognition. The rationale driving the current report is that early modulations in fMRI activity may reflect faulty evidence gathering, whereas late modulations may reflect the presence of performance monitoring mechanisms. We tested this possibility by comparing fMRI activity on correct and error trials in regions of interest (ROIs) that were selected a priori. We found pre- and postrecognition accuracy-dependent modulation in different sets of a priori ROIs, suggesting the presence of dissociable error signals. ■

INTRODUCTION

Visual object recognition is typically accomplished rapidly and with tremendous flexibility in terms of stimulus quality, orientation, and appearance (Logothetis & Sheinberg, 1996). For example, although most objects in our visual world are occluded by other objects, we have little trouble recognizing them (Johnson & Olshausen, 2005). Although often rapid, decisions about object identity involve a sequence of neural processing stages, including stimulus input, perceptual analysis, recognition, and response. Performance monitoring functions identify erroneous responses and adjust future behavior. All of these stages can be influenced (positively or negatively) by expectations in the form of top–down control (Gazzaley, Cooney, McEvoy, Knight, & D'Esposito, 2005; Bar, 2003; Miller & Cohen, 2001; Frith & Dolan, 1997; Corbetta, Miezin, Dobmeyer, Shulman, & Petersen, 1991; Fuster, 1989). Theoretically, perceptual decisions are reached after a period of evidence gathering in which information about possible response options is accumulated over time. For example, in accumulator models, inputs are assigned as evidence toward different response options depending on their fit with task parameters (Gold & Shadlen, 2007; Ploran et al., 2007; Usher & McClelland, 2001; Smith & Vickers, 1988; Ratcliff, 1978; Link & Heath, 1975; Audley & Pike, 1965). Presumably, faulty evidence gathering before recognition can lead to inefficient or erroneous decisions, the outcome of which may signal the need for later corrective feedback.

Our goal was to investigate the relative timing of error-related signals in the context of perceptual object identification. Given the typical speed of object recognition, our primary challenge was to temporally extend the perceptual decision process to cleanly identify timing-dependent modulations using functional magnetic resonance imaging (fMRI). Our approach was to gradually reveal pictures of objects from under a noise-occluded mask (Ploran et al., 2007; Carlson, Grol, & Verstraten, 2006; James, Humphrey, Gati, Menon, & Goodale, 2000). Initially, the mask fully occluded the pictures, and dissolved every 2 sec over 16 sec until fully revealed (Figure 1A). Participants were instructed to press a button as soon as they could recognize a picture's identity with a reasonable degree of confidence. This response estimated the time of recognition (T_R). We assessed accuracy by instructing participants to press the button again, when the stimulus was fully revealed, if their earlier recognition had been correct. If recognition was incorrect, they instead skipped making a second response. This paradigm allowed us to measure the evolving T_R-dependent blood oxygen level-dependent (BOLD) signal across the whole trial and evaluate the temporal dynamics of error signals relative to the timing of T_R.

[1]University of Pittsburgh, [2]Washington University, St. Louis, MO

Figure 1. Schematics of (A) the task paradigm and (B) the most basic information flow in perceptual recognition. During the task, a mask covering the object dissolved every 2 sec over eight discrete steps. Subjects pressed a button when they recognized the object identity, and again at Step 8 (14 sec) if their earlier recognition had been correct. The time scale depicted in (A) is not intended to precisely match the time scale in (B).
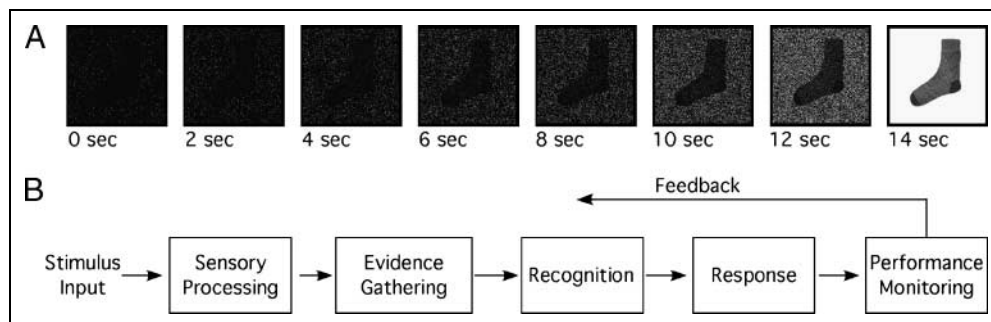
To frame our hypotheses, we consider a simple model describing the temporal flow of information through stages of perceptual recognition (Fellows, 2004; Lipshitz, Klein, Orasanu, & Salas, 2001). As shown in Figure 1B, stimulus inputs are modified by sensory processes, which in turn provide information used in perceptual recognition via feedforward connections. After a period of evidence accumulation, a decision is reached and a response is generated. The results of the decision are evaluated relative to task feedback and a priori expectations, and to adjustments to future behavior made via direct or indirect feedback connections to earlier stages of processing (e.g., Kennerley, Walton, Behrens, Buckley, & Rushworth, 2006; Debener et al., 2005; Yeung, Cohen, & Botvinick, 2004; Holroyd & Coles, 2002; Miller & Cohen, 2001). Because the scope of our study does not address the targets of feedback processing, we have depicted it ambiguously. For our purposes, the principle distinction is that evidence gathering is more prevalent than performance monitoring before the time of recognition, but that performance monitoring functions dominate following recognition. The model also does not attempt to incorporate other top–down influences such as establishment of goals, setting stimulus–response mappings, and selective attention, which we assume to be present nonetheless.

We previously reported data from this study demonstrating two distinct patterns of BOLD response that were locked to the timing of recognition (i.e., were T_R-dependent). In one set of regions, the activity increased early after trial onset and continued to increase at a T_R-dependent rate (Ploran et al., 2007). That is, activity increased more rapidly when recognition occurred early in the trial and more slowly when recognition occurred later. These "accumulator" ROIs were located in the inferotemporal (IT), posterior parietal (PPL), and dorsolateral prefrontal cortex (dlPFC). This pattern of activity is similar to the pattern of spiking rates observed in the neurophysiology literature on perceptual decision making (Gold & Shadlen, 2000, 2007; Ratcliff, Hasegawa, Hasegawa, Smith, & Segraves, 2007; Ratcliff, Cherian, & Segraves, 2003; Romo & Salinas, 2003; Cook & Maunsell, 2002; Roitman & Shadlen, 2002;

Shadlen & Newsome, 2001; Kim & Shadlen, 1999; Platt & Glimcher, 1999; Parker & Newsome, 1998; Hanes & Schall, 1996). Thus, the observed T_R-dependent response may be associated with the accumulation over time of information used in perceptual object recognition. In contrast, a second set of regions was engaged only at, or just after, the time of recognition. In these "moment-of-recognition" ROIs (or "recognition" ROIs for short), which were located near the anterior cingulate cortex (ACC), medial frontal gyrus (meFG), striatum (str), and frontal operculum near the anterior insula (aI/fO), activity remained near baseline until T_R. The BOLD response in these ROIs was characterized by a markedly transient response, which was significantly shorter than the accumulation response. We used the term "moment of recognition" as a generic term referring to any processes engaged at or after (but not before) recognition (e.g., error commission, error detection, attention, performance monitoring and adjustment...etc.).

We now examine accuracy-dependent modulations in "accumulator" and "recognition" ROIs in the context of the model depicted in Figure 1B. Our aim was to characterize the accuracy-dependent response to determine whether erroneous recognition was associated with pre- or postrecognition modulations in the BOLD response. If the function of a region (e.g., accumulator ROI) is related to gathering information used in a decision, then accuracy-dependent modulations should occur early in the trial, before recognition. Early modulations might then reflect faulty evidence gathering. In contrast, if the function of a region involves performance monitoring, then accuracy-dependent modulations should occur late in the trial, following recognition. To test these hypotheses, we examined the temporal evolution of fMRI activity on correct and error trials in accumulator and recognition ROIs.

METHODS

Subjects

Participants were 18 right-handed, native English speakers with normal or corrected-to-normal vision. Three

participants were excluded from analysis due to excessive movement and two were excluded due to data loss. Of the remaining 13 participants, eight were women; ages ranged from 20 to 30 years (mean = 24.9 years). One subject was excluded from imaging analyses due to missing cell values in the analysis of variance (ANOVA) models (too few error trials). One run from each of three participants was excluded due to excessive movement. Informed consent was obtained in a manner approved by the Institutional Review Board of the University of Pittsburgh and participants received $75.

Stimuli

Picture stimuli were drawn from a pool of 233 grayscale images (Rossion & Pourtois, 2004) that were reformatted into a standard 284 × 284 pixel image with a white background. The pictures represented ordinary, easily recognizable objects such as a ball, tie, butterfly, dog, and so forth. Five images were reserved for a practice session. Five lists of 20 pictures were randomly selected from the remaining 228 pictures. Each list was presented in a separate run of image acquisitions. Each subject received a randomly selected and ordered set of lists. The images subtended an average 10.3° of the visual field and were presented against a black background.

Behavioral Paradigm

Testing was conducted over five runs (20 trials per run) using a perceptual recognition task. Runs were randomly intermixed with five runs of a related word recognition task, which is not reported here. Each trial was 16 sec in duration and stimuli were gradually revealed from under a mask across the full length of the trial (Figure 1A). Stimulus revelation occurred regularly over eight discrete steps (2 sec per step), each corresponding with the acquisition of a whole-brain image. Trials (but not steps) were jittered to allow event-related analysis of individual trial types, with 2, 4, or 6 sec (mean ITI = 4 sec) of central fixation following each trial.

At the beginning of each trial, pictures were completely covered by a black mask. The mask partially dissolved at each of eight successive 2-sec intervals (i.e., revelation step) until pictures were completely revealed. Participants pressed a button when they could identify the picture with a reasonable degree of confidence (T_R). Neither speed nor accuracy were emphasized in the T_R response. Participants were not specifically encouraged to respond prior to full revelation, but only if and when they could identify the picture. When stimuli were fully revealed, participants pressed the same button again if their earlier recognition had been correct (VoA), but not otherwise. To factor out basic lateralized motor signals in group analyses, response hand was counterbalanced across participants (Thielscher & Pessoa, 2007).

PsyScope X was used for stimulus presentation and data collection (Cohen, MacWhinney, Flatt, & Provost, 1993; http://psy.ck.sissa.it).

Image Acquisition

Images were obtained using a Siemens Allegra 3-T scanner. Stimuli were generated on an Apple iBook G4 with PsyScope X and projected, via a mirror attached to the head coil, onto a screen positioned at the head of the magnet bore using a Sharp PG-M20X digital multimedia projector. Earplugs dampened scanner noise. Responses were made using a fiber-optic button stick connected to the computer via an interface unit (Current Designs, Philadelphia, PA).

Anatomic images were collected using an MP-RAGE sequence (repetition time [TR] = 1540 msec, echo time [TE] = 3.04 msec, flip angle = 8°, interval time [TI] = 800 msec, delay time [TD] = 0 msec). A series of whole-brain, spin-echo, echo-planar T2*-weighted functional images sensitive to the BOLD contrast (TR = 2000 msec, TE = 30 msec, flip angle = 79°, 2.2 × 2.2 in-plane resolution) were collected during testing. The first three image acquisitions were discarded to allow net magnetization to reach steady state.

Data Analysis

Analysis of Behavioral Data

Because we were interested in evaluating how recognition timing influenced the BOLD response profile, we first sorted trials according to recognition timing (T_R). Trials were sorted into 2-sec bins beginning at time 0 sec (Step 1) and proceeding through time 14 sec (Step 8). This resulted in 8 bins of 2 sec width, T_R1–8. Each bin was thus associated with a complete whole-brain image acquisition, providing one timepoint of MR data per step of revelation. Trials were then sorted by self-reported accuracy as indicated at the VoA stage. This process was limited to trials in T_R1–7, because recognition responses occurring in T_R8 took place when the stimulus was fully revealed. T_R1–7 trials receiving a later VoA response were scored as accurate trials, whereas those not receiving a later VoA response were scored as error trials. Trials receiving the first response at T_R8 ("end-trial recognition") were scored separately and were not further categorized by accuracy.

Analysis of Imaging Data

Functional images from each subject were preprocessed to remove noise and artifacts: (a) correction for movement within and across runs using a rigid-body rotation and translation algorithm (Snyder, 1996), (b) whole-brain normalization to a common mode of 1000 (Ojemann et al., 1997), and (c) temporal realignment (using sinc

interpolation) of all slices to the temporal midpoint of the first slice, accounting for differences in the acquisition time of each slice. For group analyses, functional data were re-sampled into 2-mm isotropic voxels and transformed into stereotaxic atlas space (Talairach & Tournoux, 1988). Atlas registration involved aligning each subject's T1-weighted image to a custom atlas-transformed (Lancaster et al., 1995) target T1-weighted template using a series of affine transforms (Fox, Snyder, Barch, Gusnard, & Raichle, 2005; Michelon, Snyder, Buckner, McAvoy, & Zacks, 2003).

Preprocessed data were analyzed at the voxel level using a general linear model (GLM) approach (Miezin, Maccotta, Ollinger, Petersen, & Buckner, 2000; Friston, Jezzard, & Turner, 1994). The specific implementation of this approach has been described by Ollinger, Corbetta, and Shulman (2001) and Ollinger, Shulman, and Corbetta (2001). Image processing and analyses were carried out using in-house software. Briefly, events were entered into the model according to the timing and accuracy criteria described in the previous section. Estimates of the time course of effects were derived from the model for each response category by coding 16 timepoints immediately following the onset of each trial. We included 15 event regressors in each participant's GLM, with an additional trend term to account for linear drift across a run, and a constant term to estimate the baseline signal. The 15 events included correct and error T_R1–7 trials, and end-trial-recognition events. Event-related effects are de-scribed in terms of a time series of delta functions rep-resenting the percent signal change, defined as signal magnitude divided by a constant term, at each timepoint. This approach makes no assumptions about the shape of the BOLD response. It does assume, however, that the BOLD responses for all events comprising a category are the same (e.g., all T_R7 incorrect trials elicit the same response in a voxel) and that overlapping signals summate linearly.

Hypothesis-driven Analysis

Statistical analyses proceeded in two stages, with a group of hypothesis-driven analyses followed by an ex-ploratory voxelwise analysis. First, we ran a targeted analysis on two sets of ROIs (Ploran et al., 2007) chosen a priori because of their separable contributions to object recognition (see Table 1). The procedure used to define ROIs is described in detail in our previous report (Ploran et al., 2007), and included a separate ex-periment in which we contrasted activity associated with T_R with activity associated with VoA. Voxels were includ-ed in an ROI only if they passed multiple comparison (using a voxel extent [$n = 45$] threshold of $p < .05$) and sphericity corrections. Eleven a priori accumulator ROIs were located in or near the IT, PPL, and dlPFC. We dis-carded two ROIs in cerebellum, included in the previous report, due to the observation of unusually delayed re-sponses in the ROIs relative to the other accumulator ROIs (see Figure S1 in Ploran et al., 2007). Note that including the ROIs in the region-type analyses reported below does not change the absolute significance of the results, although it does decrease the p values slightly. Fourteen a priori moment-of-recognition ROIs were lo-cated in or near the ACC, meFG, caudate nucleus, thala-mus, and aI/fO.

If erroneous decisions are based on faulty feedforward processing, then activity should differ between correct and error trials early in the trial, before the recognition decision (T_R). Notably, accuracy-dependent differences may occur after recognition because new information becomes available as the trial progresses, allowing for further accumulation. In contrast, feedback process-ing should occur only after recognition has occurred. If regions are involved in feedback processing, then accuracy-dependent modulations should follow (but not necessarily precede) recognition.

From each ROI listed in Table 1, we extracted two sets of BOLD time courses across 16 timepoints. In the T_R-*dependent set*, we were interested in identifying whether activity was dependent upon the timing of rec-ognition. If so, then the BOLD response should shift in time as T_R increases. We extracted time courses for T_R3–7, collapsing across correct and error trials to pro-duce five time courses. In the *accuracy-dependent set*, we were interested in examining whether differences in the accuracy of responding produced modulations in the pattern of time course. Because there were relatively few error trials in each T_R bin, and we wanted to con-strain the range of response times, maximal power could be achieved by averaging across all levels of T_R. How-ever, this approach would produce substantial temporal blurring (8 sec). We therefore selected the two neigh-boring bins with the most total recognition responses (T_R6 and T_R7), collapsed them into a single condition (T_R6 + 7), and extracted time courses for correct and error trials to obtain two accuracy-dependent time courses. We used this approach because the number of error trials at each T_R (Table 2) limited the power to test for interactions across each level. To test T_R-*dependence* in the BOLD responses, we computed repeated mea-sures ANOVAs on the full time-course data from each ROI, averaged over all voxels in the ROI, with five levels of T_R and 16 levels of time. We set the alpha level for significance at $p < .05$, and trend at $.05 < p < .10$.

To test the reliability of *accuracy-dependent differ-ences*, we performed two separate single-factor repeated measures ANOVAs on a subset of the time-course data from each ROI. In each ANOVA, there were two levels of accuracy (correct, error) and three levels of time. The first ANOVA targeted the prerecognition epoch by ex-amining timepoints 6–8, corresponding with 10–14 sec from trial onset. This window encompasses the time just prior to perceptual recognition decisions occurring at T_R6–7. Due to averaging, it also necessarily encom-passes 2 sec of postrecognition time at T_R6. However,

Table 1. List of Hypothesis-driven ROIs, Atlas Coordinates, and Statistical Outcomes

#	~Anatomic Location	Hem.	~BA	x	y	z	p6–8	p10–12
A Priori Accumulator ROIs								
1	Inferior occipital gyrus 2a	L	18	−32	−89	−9	**.016**	.566
2	Middle occipital gyrus	L	19	−30	−78	21	.197	.070
3	Superior occipital gyrus	R	19/39	31	−71	29	**.025**†	.339
4	Fusiform gyrus	R	37	49	−61	−9	**.038**†	.380
5	Fusiform gyrus	L	20	−31	−39	−14	.124	.967
6	Fusiform gyrus	L	37	−42	−63	−9	.096	**.012**
7	Intraparietal sulcus 2b	L	7/19	−26	−68	38	**.011**	**.001**
8	Middle frontal gyrus	L	46	−44	28	24	.175	**.001**
9	Middle frontal gyrus	R	46	47	32	19	.113	.535
10	Post. inf. frontal gyrus	L	9/6	−46	0	32	.562	**.027**
11	Inferior frontal gyrus	R	6/9	44	6	33	**.039**†	**.001**
A Priori Recognition ROIs								
12	Inferior parietal lobule	R	7	34	−57	47	.416	**.006**
13	Inferior parietal lobule	R	40	49	−48	47	.718	**.006**
14	Thalamus	L	NA	−11	−12	8	.083†	**.038**
15	Thalamus	R	NA	11	−13	9	.621	.168
16	Striatum	L	NA	−11	7	5	.844	**.037**
17	Striatum	R	NA	12	6	3	.779	.582
18	aI/fO	R	13	33	22	−2	.858	**<.001**
19	aI/fO	L	13	−32	22	1	**.011**†	**<.001**
20	Anterior cingulate	R	32	6	24	31	.864	**.003**
21	Dorsal anterior cingulate	R	8	1	26	42	.595	**<.001**
22	Medial frontal gyrus	L	6	−1	14	51	.544	**<.001**
23	Inferior frontal gyrus	L	47	−42	19	1	.378	**.001**
24	Inferior frontal gyrus	R	47	45	14	−3	.383	**.002**
25	Precentral gyrus	R	44	51	15	7	.097†	**.019**

\# = ROI number; Hem. = hemisphere; BA = ~Brodmann's area; *x*, *y*, *z* = atlas coordinates; *p*6–8 = probability in the prerecognition accuracy-dependent analysis; *p*10–12 = probability in the postrecognition accuracy-dependent analysis; † = *p* value for interaction of accuracy with time, otherwise *p* values are from the main effect of accuracy; *p* values in bold text < .05.

with an assumed 2–3 sec lag in the onset of the BOLD response, and a 4–6 sec lag in the time-to-peak (Miezin et al., 2000), activity in this time window should be almost exclusively related to processing prior to recognition. The second ANOVA targeted the postrecognition epoch by examining timepoints 10–12, corresponding with 18–22 sec from trial onset. This time window occurs after recognition and after the stimulus is fully revealed.

Table 2. Total Number of Recognition Responses, Sorted by Accuracy and Binned Time of Recognition

	T_R1	T_R2	T_R3	T_R4	T_R5	T_R6	T_R7	ETR
Correct	1 (0.29)	16 (1.50)	71 (3.85)	157 (5.35)	156 (2.52)	247 (5.33)	204 (7.52)	163 (8.00)
Error	1 (0.29)	4 (0.78)	8 (1.07)	24 (2.26)	32 (1.92)	39 (2.38)	25 (1.24)	NA

T_R = binned time of recognition; ETR = end-trial recognition; NA = not applicable; standard deviations ($n = 13$) are listed in parentheses.

All reported anatomic labels and Brodmann's areas (BA) are approximate.

Exploratory Analysis

We also ran exploratory voxelwise analyses to identify voxels in which activity modulated as a function of accuracy in the pre- and postrecognition epochs. We conducted these analyses because the ROIs were defined, in a separate experiment (Ploran et al., 2007), without considering incorrect responses. Thus, in our current ROI analyses, we may overlook voxels showing accuracy-dependent effects. Group z-statistical maps were derived from the GLMs using voxelwise repeated measures ANOVA (Winer, Brown, & Michels, 1991), with time as a repeated factor with three levels. The ANOVA implementation in FIDL produces a set of main effect and interactions images determined by the factors in the design (Ollinger, Corbetta, et al., 2001; Ollinger, Shulman, et al., 2001). The main effect of time image identifies voxels in which the temporal profile over the analyzed time period is not flat (i.e., no change in signal from the baseline constant term). Interaction by time images identify voxels in which activity differs across levels of factors as a function of time. Images were smoothed with a Gaussian spatial filter (4 mm full width at half maximum) during analysis.

RESULTS

Behavioral Results

Recognition responses were spread across the trial, with most responses occurring in the second half. The numbers of recognition responses, broken down by accuracy and T_R bin, are listed in Table 2. Overall, most responses occurred at T_R6 and 7. At T_R3 there was a substantial number of total trials (79), but there were too few trials at T_R1 and T_R2 to include in imaging analyses. A total of 163 trials were categorized as "end-trial recognition." Because these trials were associated with only a single manual response, they were not included in the analyses.

Imaging Results

Dependency of BOLD Signal on Recognition Timing

In this analysis, we evaluated T_R-dependence of activity in accumulator and recognition ROIs by entering the time-course data from each ROI into a one-way repeated measures ANOVA, with five levels of T_R (3, 4, 5, 6, 7) and 16 levels of time. Unlike our previously reported findings (Ploran et al., 2007), the data in this analysis were collapsed over correct and error trials. Still, all of the ROIs displayed a significant interaction of T_R and time [all $F(60, 660) > 1.41$, $p < .05$], indicating that the shape of the BOLD response changed reliably across levels of

T_R. Time courses from eight ROIs are displayed in the middle panels of Figures 2 and 3, plotted in gray scale. These eight ROIs showed a clear separation in the rising edge of the BOLD response across levels of T_R, with approximate 2-sec steps in the peak of activity, which was time-locked with the different levels of T_R.

ROIs in the accumulator group (Figure 2) displayed an early onset of activity followed by a gradual T_R-dependent buildup of activity, peaking about 4 sec after each T_R bin. This pattern of response is consistent with an accumulation of information prior to the time of recognition (Ploran et al., 2007). As shown in Figure 2, the slopes of the leading edges of the BOLD response became more shallow as T_R increased from Steps 3 to 7.

In contrast to the early onsets observed in the posterior ROIs, frontal regions including the meFG, the ACC, and the aI/fO, tended to display a T_R-dependent onset of activity such that activity increased at the time of recognition. For example, in Figure 3A–C, note the time course for the T_R7 condition (in black) in the medial frontal ROIs and in the right aI/fO. Activity remains near baseline until the seventh timepoint, and only then begins to increase at $\sim T_R$. This pattern of response indicates that these regions play very little role in prerecognition processing. Instead, they become active near the time when a decision has been reached.

Pre- and Postrecognition Accuracy-dependent Effects

To test the possibility that ROIs modulated according to recognition accuracy, we entered the combined $T_R6 + 7$ data from each ROI into two analyses on a subset of the 16 timepoints. A repeated measures ANOVA on timepoints 6–8 targeted the prerecognition period to examine possible feedforward performance-related modulations. A repeated measures ANOVA on timepoints 10–12 targeted a postrecognition period to examine possible feedback performance-related modulations. Each ANOVA model included two levels of the factor accuracy (correct, error) and three levels of time. Importantly, because only three timepoints were considered in each analysis, we considered any main effect of accuracy or interaction of time with accuracy in the prerecognition epoch as evidence for accuracy-dependent feedforward effects. Accuracy-dependent feedback effects were also noted by a main effect of accuracy or a Time by Accuracy interaction in the postrecognition epoch.

Pre- and Postrecognition Activity in A Priori Accumulator ROIs

We first examined pre- and postrecognition activity in the accumulator ROIs. In all ROIs except one located near the left fusiform gyrus (Table 1, ROI 5), activity at timepoints 6–8 was greater on error than on correct trials. Analysis of the activity in this prerecognition

Figure 2. Four a priori accumulator ROIs and their T_R-dependent (middle panels) and accuracy-dependent (far right panels) time courses. ROIs are projected over a backdrop of the anatomic template used in atlas transformation. Atlas x, y, z coordinates are listed below each ROI. In the graphs, signal change percentage from baseline is plotted as a function of time. T_R-dependent responses for the five conditions are plotted over the entire trial plus 16 sec to capture the tail of the BOLD response. The T_R conditions are associated with graded gray-scale values (see key). The corresponding time bin for each T_R is denoted by a gray bar above the x-axis. The black bars spanning timepoints 12 and 20 denote the pre- and postrecognition epochs. Shaded areas represent a significant effect of accuracy in the time window encompassing the pre- and postrecognition epochs. (A) ROI near the left IPS (Table 1, #7). (B) ROI near the left IOG (Table 1, #1). (C) Right lateral FG (Table 1, #4). (d) ROI near the right SOG (Table 1, #3).
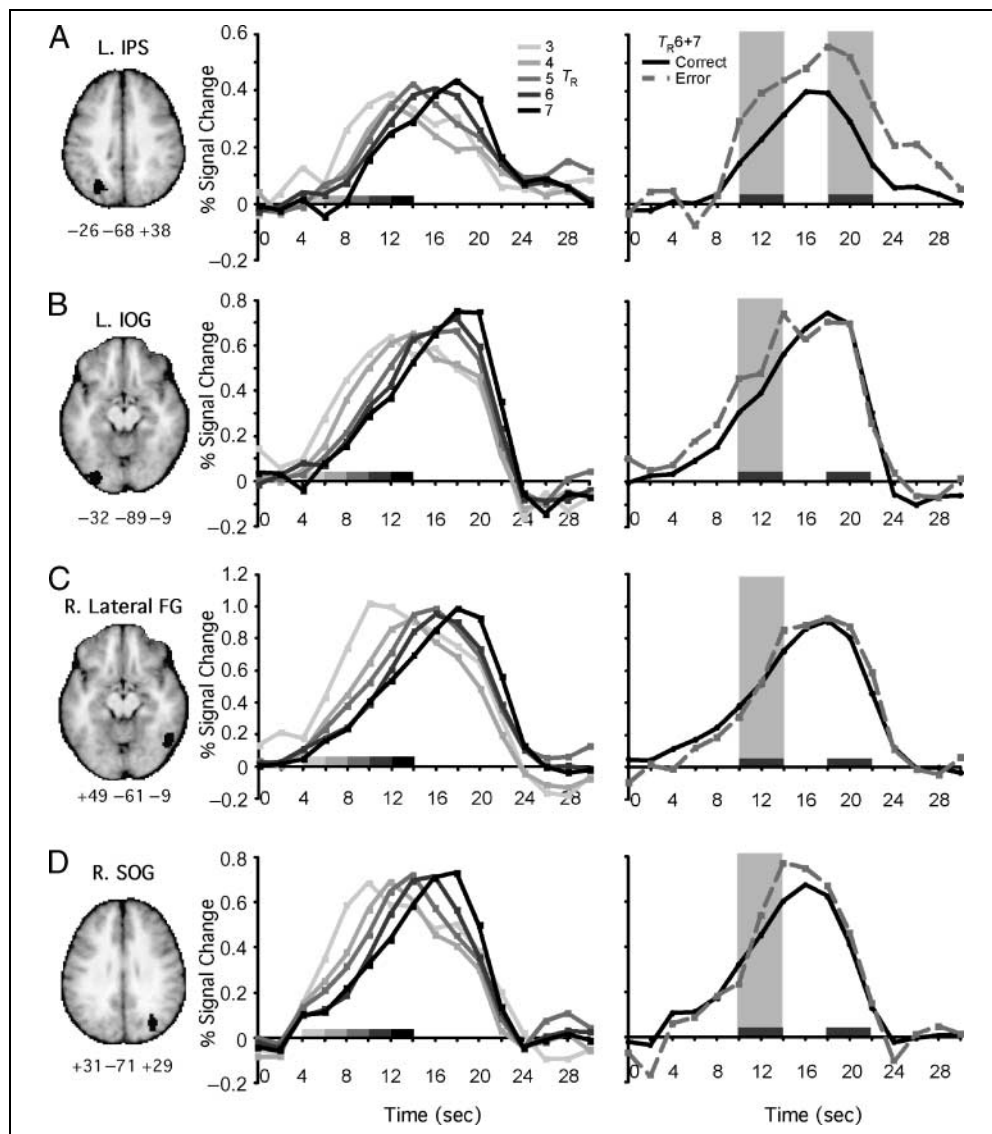
epoch identified two ROIs, located near the left inferior occipital gyrus (IOG; Table 1, #1; Figure 2A) and the left intraparietal sulcus (IPS; Table 1, #3; Figure 2B), that displayed a significant main effect of accuracy in the prerecognition epoch [$F(1, 12) = 7.87, 9.13$, respectively; both $p < .05$]. In Figure 2, far right panels, prerecognition epochs with significant accuracy-dependent effects are signified by a shaded area. The IPS region [$F(1, 12) = 17.18, p < .05$], but not the IOG region [$F(1, 12) = 0.35, p > .10$], also displayed a significant main effect of accuracy in the postrecognition epoch. Three ROIs, located in or near the right superior occipital gyrus (SOG; Table 1, #3), right lateral fusiform gyrus (FG; Table 1, #4), and right IFG (Table 1, #11), displayed an interaction of accuracy and time [$F(2, 24) = 4.35, 3.77$, and 3.73, respectively; all $p < .05$]. The postrecognition ANOVA for these three ROIs revealed a significant main effect of accuracy only in the IFG [$F(1, 12) = 17.14, p < .01$]. One additional ROI, located near the

left lateral FG (Table 1, #6), displayed a marginally significant main effect of accuracy in the prerecognition epoch [$F(1, 12) = 3.27, p = .096$]. This effect was also significant in the postrecognition epoch [$F(1, 12) = 8.77, p < .05$]. None of the five remaining accumulator ROIs approached significance in the prerecognition epoch.

Postrecognition activity differed either marginally or significantly on correct versus error trials in ROIs in the left middle occipital gyrus (MOG; Table 1, #2), the middle frontal gyrus (MFG; Table 1, #8), and the posterior IFG (Table 1, #10). In Figure 2, far right panels, time courses from four of the ROIs are displayed as a function of response accuracy. Figure 2A–B shows ROIs near the left IPS and the left IOG in which prerecognition activity was reliably greater on error than correct trials. Figure 2C–D shows ROIs in the right lateral fusiform and the right SOG in which activity was initially [i.e., timepoint 5 (10 sec)] less on error than on correct

Figure 3. Four a priori feedback ROIs and their T_R-dependent (middle panels) and accuracy-dependent (right panels) time courses. Details are the same as described in Figure 2. (A) ROI in the left medial frontal gyrus near pre-SMA (Table 1, #22). (B) Bilateral dACC (Table 1, #21). (C) Left IFG (Table 1, #23). (D) Right aI/fO (Table 1, #18).
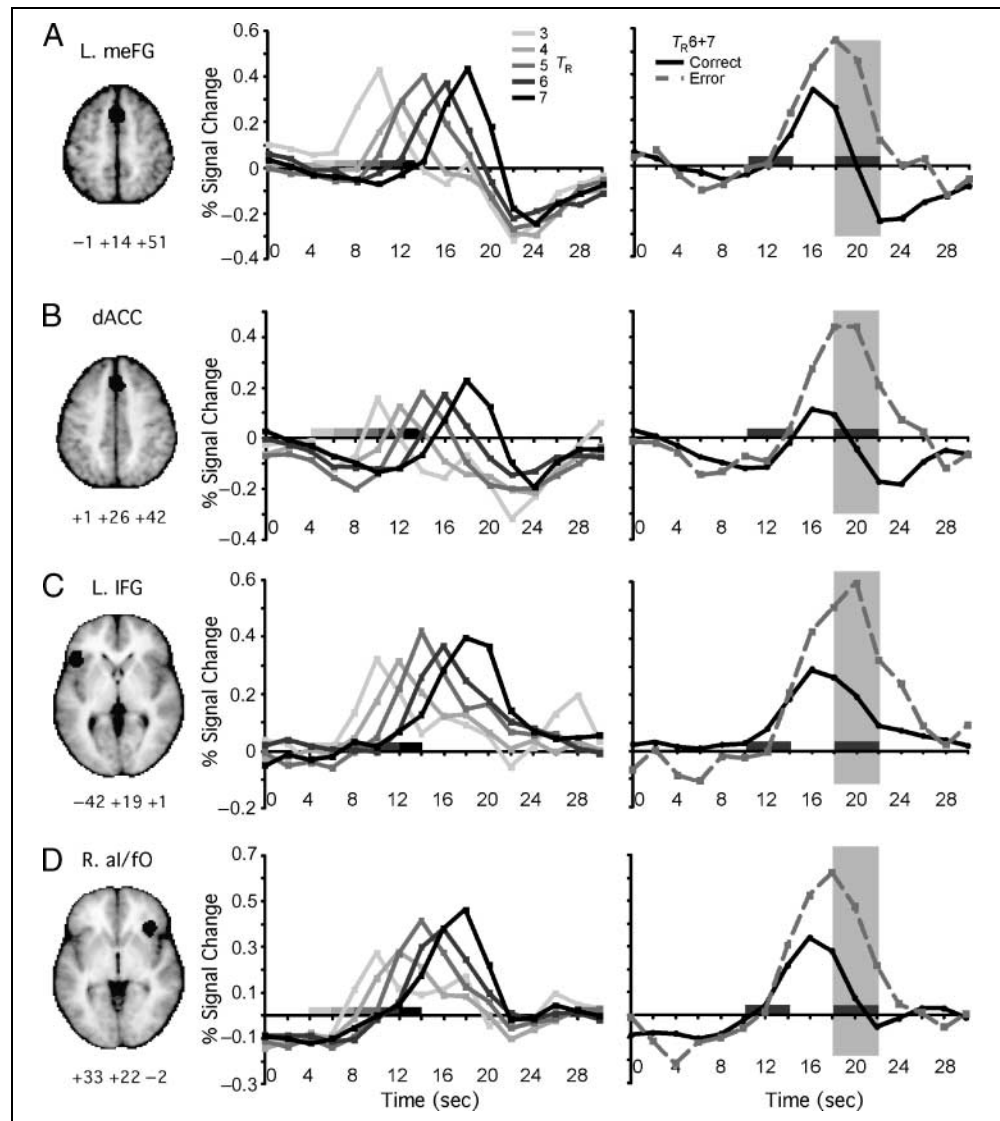
trials. However, by timepoint 7 (14 sec), activity was reliably greater on error than on correct trials, indicating a crossover interaction during the prerecognition epoch. Of these ROIs, the left IPS also displayed an accuracy-dependent effect in the postrecognition epoch (Figure 2A, red shaded area).

Overall, 5 of the 11 accumulator ROIs reliably modulated according to accuracy (error > correct in all cases) in the prerecognition epoch. One additional ROI showed a trend toward a reliable accuracy-dependent effect. A total of five ROIs modulated according to accuracy in the postrecognition epoch, with one additional ROI showing a trend.

Pre- and Postrecognition Activity in A Priori Moment of Recognition ROIs

Of the 14 a priori moment-of-recognition ROIs, only the left aI/fO (Table 1, #19) displayed a significant effect of accuracy in the prerecognition epoch [Accuracy by

Time: $F(2, 24) = 5.46, p < .05$]. The time-course data from this ROI are not shown, but are similar to the analogous right aI/fO ROI displayed in Figure 3D. In two additional ROIs located in the left thalamus (Table 1, #14) and near the right precentral gyrus (Table 1, #25), prerecognition modulations were marginally significant [Accuracy by Time: $F(2, 24) = 2.77, 2.57$, respectively; both $.05 < p < .10$].

In contrast, 12 of the 14 ROIs displayed a significant main effect of accuracy in the postrecognition epoch (see Table 1; all $F > 5.44, p < .05$). Accuracy-dependent activity for $T_R 6 + 7$ from four of the ROIs is displayed in Figure 3. Included are ROIs in the medial frontal lobes near the presupplementary motor area [pre-SMA] (BA 6; Figure 3A), the dorsal ACC near BA 6 (Figure 3B), the left IFG near BA 47 (Figure 3C), and the right aI/fO near BA 13 (Figure 3D). The presence of significant postrecognition accuracy effects is denoted by a shaded area. Thus, the predominant finding from this set of analyses was that in the moment-of-recognition ROIs,

accuracy-dependent modulations were observed mostly in post- but not prerecognition epochs.

ROI Dependency of Pre- and Postrecognition Accuracy Effects

To determine whether accumulator and recognition ROIs differed in terms of the accuracy-dependent effects, we averaged the activity on correct and error trials across the three timepoints in each epoch to produce two values for each ROI (correct, error) for each epoch. The averaged timepoint data are plotted in Figure 4, which displays percent signal change as a function of epoch (pre, post), accuracy (correct, error), and region type (accumulator, recognition). We chose to use all a priori ROIs in each group rather than select just those showing reliable pre- or postrecognition effects in order to draw an unbiased comparison between the two ROI groups. As shown in Figure 4, activity was greater in accumulator than in recognition ROIs. To test the reliability of findings in each epoch, we entered the pre- and postrecognition data into two 2-accuracy (correct, error) by 2-region-type (accumulator, recognition) ANOVAs, with accuracy as a repeated measure and region type as a between factor. Because we did not have a priori predictions involving a comparison of pre- and postrecognition activity, we did not include epoch as a factor in the model.

The prerecognition analysis revealed main effects of accuracy [$F(1, 23) = 12.56, p < .005$] and the between factor region type [$F(1, 23) = 64.33, p < .0001$], indicating that at timepoints 6–8, activity was greater on error than correct trials, and was greater in accumulator than in recognition ROIs (Figure 4, PRE-RECOG). Importantly, the interaction of accuracy by region type also reached significance [$F(1, 23) = 8.22, p < .01$], indicat-

ing that the accuracy-dependent effects (error > correct) were greater in accumulator than in recognition ROI groups.
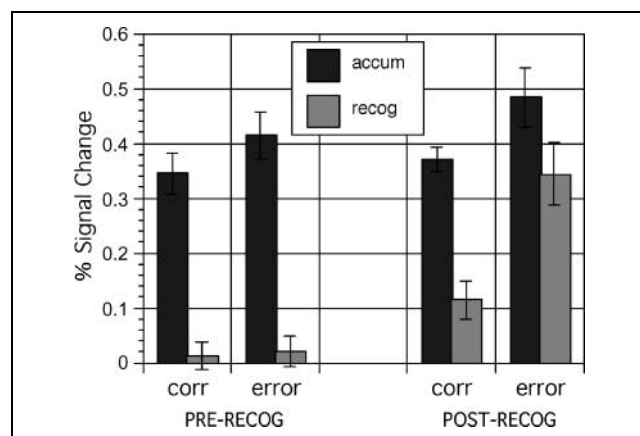
The postrecognition analysis produced a similar pattern of results, with significant main effects of accuracy [$F(1, 23) = 53.60, p < .0001$] and region type [$F(1, 23) = 13.18, p = .001$]. The interaction of accuracy by region type was also reliable [$F(1, 23) = 6.84, p < .05$]. In contrast to the prerecognition results, the analyses indicated that the accuracy-dependent effects (error > correct) observed in recognition ROIs were greater than in accumulator ROIs (Figure 4, POST-RECOG). Because the differences between a priori ROI groups were significant, we will discuss effects at the ROI group level. However, it is important to emphasize that because some ROIs failed to show reliable effects at the region level (Table 1), it will likely be useful to ultimately consider a finer-grain analysis and characterization of specific patterns.

The Timing of Error Signals

Although we have thus far focused on specific epochs in the time course of BOLD activity, the recognition process occurred dynamically across the trial. To evaluate accuracy-dependent signals in accumulator and recognition ROIs, we computed the error minus correct difference (''error signal'') in each ROI across all 16 timepoints, then averaged over all ROIs in each region group. These data are displayed in Figure 5A. Data points falling above the 0% signal change line reflect more activity on error than correct trials, whereas data points below 0% reflect less activity on error than correct trials. The error signal in accumulator ROIs separated from 0% at timepoint 8 sec (Step 5 of revelation), and extended throughout most of the trial. In contrast, the error signal in moment-of-recognition ROIs began at timepoint 14 sec. The pattern that emerges from this view of the data is that early in the trial, prior to recognition, the error signal is carried by accumulator ROIs. However, beginning at VoA at 14 sec, the error signal becomes dominated by the moment-of-recognition ROIs.

This relationship is illustrated in Figure 5B, which displays the timepoint-by-timepoint difference in error signal between the two ROI groups (accumulator − recognition). Positive and negative data points reflect error signals predominantly arising from accumulator and recognition ROIs, respectively. Timepoints 10–14 sec correspond with the prerecognition epoch, whereas timepoints 18–22 correspond with the postrecognition epoch.

Exploratory Voxelwise Analyses

We next conducted the pre- and postrecognition accuracy-dependent analyses at the voxel level in order to identify whether the ROI analyses missed areas showing

Figure 4. Mean signal change in pre- and postrecognition epochs plotted as a function of epoch, accuracy (correct, error), and region type (accumulator, recognition). Signal change values were averaged across the three timepoints in each epoch. Error bars denote standard error of the mean.
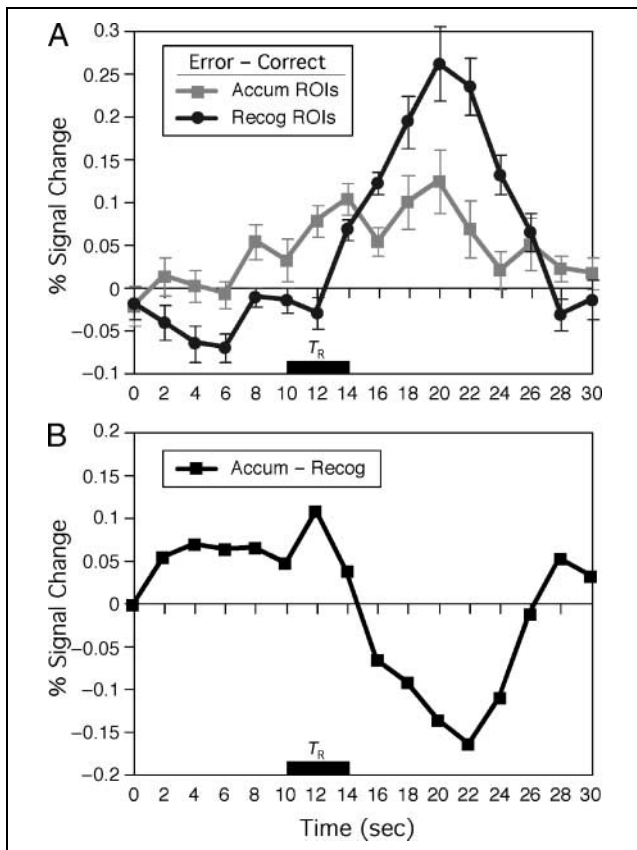
Figure 5. Difference time courses are plotted in units of percent signal change as a function of time. VoA marks the time at which the stimulus was fully revealed. (A) Error minus correct differences (error signals) are plotted according to the region type, with accumulator ROI data in gray and recognition ROI data in black (with *SEM* bars). Positive values reflect error > correct activity, whereas negative values reflect correct > error activity. (B) This graph depicts the difference in error signals between accumulator and recognition ROIs as a function of time. Positive and negative values reflect greater error signals in accumulator and recognition ROIs, respectively.

accuracy-dependent effects. In two repeated measures ANOVAs with one factor of accuracy (correct, error) and three levels of the repeated measure time, we identified voxels in which activity differed on correct and error trials. In the prerecognition analysis, we used data from timepoints, whereas in the postrecognition analysis, we used timepoints 10–12. Because of the exploratory nature of the paradigm and the relatively low numbers of error trials overall, we set the threshold to $z > 2.2$ ($p < .014$, two-tailed).

As displayed in Figure 6A, activity in regions in or near the FG ($\sim$BA 37), the IOG ($\sim$BA 18), the middle temporal gyrus (MTG, $\sim$BA 21), the lateral inferior parietal lobule (IPL $\sim$BA 39), the cuneus (Cu $\sim$BA 18), and the posterior intraparietal sulcus (pIPS $\sim$BA 7) differed across the three timepoints included in the analysis (main effect of accuracy). Worth mentioning here is that the left aI/fO, which demonstrated a significant inter-

action of accuracy by time in the prerecognition epoch, is absent from this main effect image. It is present at near to subthreshold levels in the interaction image (not shown). Functional data are projected over a backdrop of the anatomic template used to transform data into atlas space. The atlas *z*-coordinates are displayed below each slice. Other than the MTG areas, these activations are broadly consistent with the location of our a priori ROIs.

Figure 6B shows results from the postrecognition analysis. This analysis revealed a more widespread set of modulations, including many IT and parietal areas that demonstrated accuracy-dependent modulations in the prerecognition analysis. These latter findings corroborate the finding in a priori accumulator ROIs in which modulations tended to occur in both the pre- and postrecognition epochs. In addition to these posterior ROIs, a number of lateral and medial frontal areas modulated according to accuracy. These included the bilateral aI/fO near BA 13, the meFG near BA 6, the dACC near BA 32, and the right MFG near BA 8. Other prominent activations were found bilaterally near the tail of the caudate (CT; see slice at $z = -02$ in Figure 6) and along the extent of the left IPS near BA 40/39 (Figure 6, $z = 40$). Overall, the results indicate that most of the areas showing accuracy-dependent effects were included in the ROI analyses.

DISCUSSION

In this study, we examined accuracy-dependent signals occurring prior to, during, and following perceptual object recognition. The results reinforce our prior classification involving accumulator and moment-of-recognition areas (Ploran et al., 2007) by associating each with a specific pattern of T_R-dependent performance-related signals. The present findings represent an important extension of our past report (Ploran et al., 2007) by demonstrating two types of error signal, distinguished by their timing relative to recognition. Accumulator and moment-of-recognition regions were dissociated in terms of the temporal profile of the accuracy-dependent modulations. Regions in the IT near the occipital/temporal junction ($\sim$BA 19/37) and the fusiform gyrus, middle and inferior frontal gyrus, and posterior parietal cortex were more active on error than correct trials *prior to* the time of recognition. In contrast, moment-of-recognition ROIs, located near the aI/fO, dACC, vACC, meFG, and pIFG, were more active on error than on correct trials *after* the time of recognition. Of these latter regions, only one (left aI/fO) also significantly modulated prior to recognition. Thus, in terms of functional significance, the data suggest that the early error signals arising from accumulation ROIs were related to faulty evidence about object identity, whereas the later signals arising from frontal and subcortical areas were related to the act of making an

Figure 6. Results from the exploratory accuracy-dependent analyses are displayed in horizontal sections. Functional data are projected over the average anatomic template and are color-coded according to Z-score (see key) derived from the respective main effect of time image. Shown are voxels in which activity modulated with accuracy in the pre- (A) and postrecognition (B) epochs. The Z values listed below each horizontal slice designate the level of horizontal slice in Talairach atlas coordinates (Talairach & Tournoux, 1988). aI/fO = anterior insula/frontal operculum; pIPS = posterior intraparietal sulcus; IPL = inferior parietal lobule; Cu = cuneus; MTG = middle temporal gyrus; IOG = inferior occipital gyrus; FG = fusiform gyrus; meFG = medial frontal gyrus; SPL = superior parietal lobe; dACC = dorsal anterior cingulate cortex; CT = caudate tail.
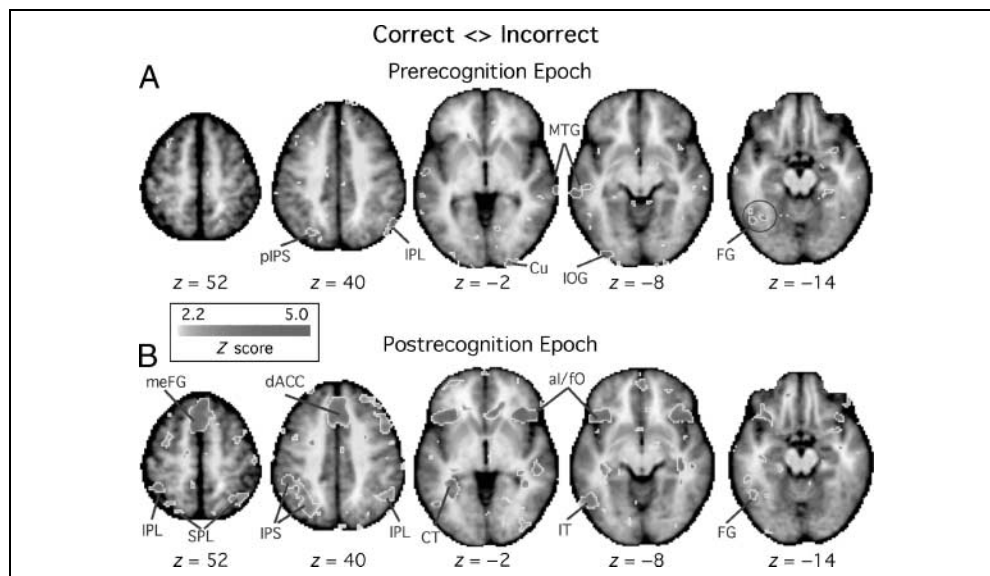
incorrect response, error detection/awareness, and/or performance monitoring and feedback.

Early Error Signals in Accumulator ROIs

The T_R-dependent pattern of accumulating signal in the 11 a priori accumulator ROIs can be explained by several accounts of information processing. The dependence of these signals on T_R, combined with an early onset and long duration of activity, has led us to believe (see Ploran et al., 2007) that this pattern could reflect an integrative "evidence accumulation" process that contributes to perceptual decisions, such as those observed in single-unit studies in nonhuman primates (Gold & Shadlen, 2000, 2007; Ratcliff et al., 2003, 2007; Cook & Maunsell, 2002; Roitman & Shadlen, 2002; Shadlen & Newsome, 2001; Kim & Shadlen, 1999; Hanes & Schall, 1996). The general finding in the neurophysiological literature is that task decisions are related to spiking rates in brain areas that are thought to accrue evidence and compute decision variables (Platt & Glimcher, 1999; Hanes & Schall, 1996). Importantly, the process of evidence gathering is time consuming and is separable from the processing of sensory inputs and the commitment to a decision (Gold & Shadlen, 2007).

Although the T_R-dependent findings are consistent with a threshold account thought to underlie decision variables, the direction of accuracy-dependent findings are harder to explain; activity was greater (i.e., increased faster) on error trials than on correct trials. A strict threshold account would predict that a faster rise in activity would trigger earlier recognition (e.g., Hanes & Schall, 1996). Yet, we found that the faster rise in activity on error trials was associated with an erroneous response that coincided with the timing of correct responses. For example, consider the prerecognition epoch in the left IPS ROI displayed in Figure 2A. At 14 sec, signal change on correct trials, at ∼0.3%, is nearing peak activity. On average, this timepoint coincides with T_R if a 2-sec lag in the BOLD response is assumed. By contrast, activity on error trials reaches 0.3% signal change ∼4 sec earlier, well before the recognition response.

What explains the early accuracy-dependent findings in accumulator ROIs? We consider two possible explanations. One alternative is that early accuracy-dependent modulations are related to top–down feedback processing related to initial hypotheses about object identity. At each step of revelation, as new stimulus information becomes available, participants could evaluate whether their hypotheses were correct or incorrect prior to generation of a T_R response. This strategy could conceivably correlate with greater activity on error trials if there were contextual or object-specific factors influencing object recognition. For example, at a particular degradation, Object A may coincidentally resemble Object B. At the

next degradation, however, Object B may be ruled out by new evidence derived from incoming sensory processing. A second alternative is that early modulations are due to an increased bottom–up load on accumulators. By this account, erroneously recognized items tended to be associated, on average, with a greater number of possible alternative solutions (even if the subject was unaware of those alternatives). The increase in alternatives consequently requires increased neural activity to track evidence for each hypothesis. Computationally, this alternative is formulated in race (e.g., Logan, 2002; Vickers, 1970; Audley & Pike, 1965) and dual diffusion models (Ratcliff et al., 2007) in which evidence accrual toward N alternatives occurs in N accumulators.

We believe that several observations support the bottom–up accumulator load explanation. First, as noted by Carlson et al. (2006), the moment of recognition ($\sim T_R$) is often subjectively experienced as occurring as a sudden transition from uncertainty to certainty. The suddenness of recognition suggests that overt hypothesis generation is not prevalent prior to recognition. A more compelling observation, however, was that only one ROI from the moment-of-recognition group (left aI/fO) demonstrated accuracy-dependent modulations prior to recognition. Many of the ROIs in this group, including the ACC and the aI/fO, have been strongly implicated in performance monitoring and task-level processing (Dosenbach et al., 2006; Botvinick, Braver, Barch, Carter, & Cohen, 2001; Carter et al., 1998; Vogt, Finch, & Olson, 1992). In fact, the signature finding from our study was that regions in the moment-of-recognition group were inactive until T_R. If feedback occurred prior to recognition, and these regions were involved in feedback processing related to performance monitoring, they should have been active prior to recognition. This was clearly not the case (see Figures 3 and 4).

Late Error Signals and Performance Monitoring

The second type of error signal, found in ROIs in or near the medial frontal gyrus, aI/fO, thalamus, striatum, posterior parietal cortex, and left IFG, occurred later in the trial. The postrecognition accuracy- and T_R-dependent modulation was exceptionally robust, despite the relatively low number of error trials. As shown in Figure 5A, there was very little variance in this signal across the 14 ROIs. Our data demonstrate that, in recognition ROIs, the error signals occurred at or after the recognition response, but were nonexistent before the response in 13 of the ROIs (Figure 4). Across all recognition ROIs, the error responses dominated late in the trial, occurring most prominently 6–8 sec after the object was fully revealed at VoA (Figure 5; times 20–22 sec).

One factor that may have influenced activity in these ROIs was the presence of a motor response at T_R. In the monkey, medial frontal areas near the cingulum and the

SMA are involved in motor functions (Picard & Strick, 1996). The T_R-dependent data, however, show that although these ROIs exhibited robust responses associated with T_R, there was very little, if any, response associated with the overt button press at VoA (Figure 3, middle panels). This finding indicates that the ROIs were not obligatorily recruited during generation of motor output, but instead that processing was related to the cognitive events involved in perceptual recognition. In support of this view, the largest increases in signal change occurred on error trials, which were signified by the *absence* of a button press at VoA.

The timing of activity supports the view that these ROIs may be involved in error detection and correction functions related to performance monitoring, which is in accord with many existing accounts of ACC and pre-SMA function (Hampton & O'Doherty, 2007; Thielscher & Pessoa, 2007; Dosenbach et al., 2006; Fleck, Daselaar, Dobbins, & Cabeza, 2006; Grinband, Hirsch, & Ferrera, 2006; Brown & Braver, 2005; Sanfey, Rilling, Aronson, Nystrom, & Cohen, 2003; Braver, Barch, Gray, Molfese, & Snyder, 2001; Botvinick, Nystrom, Fissell, Carter, & Cohen, 1999; Rogers et al., 1999; Bush et al., 1998; Dehaene, Posner, & Tucker, 1994; Vogt et al., 1992; Posner & Petersen, 1990; Posner, Petersen, Fox, & Raichle, 1988). The late error signal may be associated with the error-related negativity (ERN) observed following overtly incorrect responses (Yeung et al., 2004; Falkenstein, Hohnsbein, Hoormann, & Blanke, 1991). ERP studies of error processing have demonstrated a prominent negative signal (the ERN) beginning near the time of the erroneous response and developing over several hundred milliseconds (Coles, Scheffers, & Holroyd, 2001; Falkenstein, Hoormann, Christ, & Hohnsbein, 2000). The source of the ERN appears to be the ACC (Debener et al., 2005; Yeung et al., 2004). In our task, because stimuli were fully revealed at the end of each trial, subjects were eventually given feedback regarding the accuracy of recognition. Thus, they became aware of the error at least by the end of the trial, and perhaps earlier as new information became available. In our analysis of $T_R 6 + 7$, error awareness could occur at any time between recognition and the end of the trial. Accordingly, the possible onset of awareness corresponds well with the onset of the BOLD response (between 12 and 14 sec from trial onset) in "recognition" ROIs (Figure 5A). Because we did not record the timing of error awareness, we cannot determine whether responses were related to the act of making an erroneous response (commission) or to the detection of the error. Interestingly, ERNs are larger when subjects are certain they have made an error than when uncertain (Scheffers & Coles, 2000), suggesting that the modulations in our task were related to error detection. However, because error detection could occur at any time between T_R and VoA, and commission always occurred at T_R, the BOLD responses associated with commission should be more consistent than those associated with detection.

Although there has been progress in understanding the role of the ACC in cognitive control, the current data further implicate ROIs outside the medial wall of the frontal lobes that are involved in performance monitoring, including the right IPL, thalamus, striatum, aI/fO, and portions of the bilateral posterior IFG (Menon, Adleman, White, Glover, & Reiss, 2001). It is important to emphasize that, despite the difference in the magnitude of signal change on correct and error trials, T_R-dependent modulations were observed on both correct (Ploran et al., 2007) and incorrect trials (Figure 3). This finding indicates that these areas perform a function related to the correct performance, and this function is utilized more when performance is in error. What could this function be? As we have noted, there are a number of hypotheses about ACC function, including conflict monitoring and error detection. The T_R-dependence observed on correct trials does not support a specific role in error detection. Another possibility is that activity reflects the degree of attentional capture (Posner & Rothbart, 2007; Frith & Dolan, 1997; D'Esposito et al., 1995). That is, on both correct and incorrect trials, the realization of object identity captures attention and is associated with a T_R-dependent BOLD response. However, on incorrect trials, the additional attention warranted by detecting an error is associated with a second BOLD response. In our analysis, the two responses related to attention would summate and produce a larger response on incorrect trials.

In our view, the timing of this late error signal also constrains the trial-related activity in the ACC (and other recognition ROIs), at least in this paradigm, to processing occurring at or after the decision. For example, the current accuracy-dependent analysis focused on trials in which recognition occurred late in the trial, at T_R6 and T_R7. By this stage, there was ample time to generate hypotheses and prepare responses, but activity, nevertheless, did not increase until the time of recognition. Thus, the ACC and other ROIs in the a priori recognition group appeared not to participate in predecision processes such as object classification or response selection, but instead to later processes important in performance monitoring, such as error detection or initiation of feedback (Holroyd & Coles, 2002).

REFERENCES

Audley, R. J., & Pike, A. R. (1965). Some stochastic models of choice. *British Journal of Mathematical and Statistical Psychology, 18,* 183–192.

Bar, M. (2003). A cortical mechanism for triggering top–down facilitation in visual object recognition. *Journal of Cognitive Neuroscience, 15,* 600–609.

Botvinick, M., Nystrom, L. E., Fissell, K., Carter, C. S., & Cohen, J. D. (1999). Conflict monitoring versus selection-for-action in anterior cingulate cortex. *Nature, 402,* 179–181.

Botvinick, M. M., Braver, T. S., Barch, D. M., Carter, C. S., & Cohen, J. D. (2001). Conflict monitoring and cognitive control. *Psychological Review, 108,* 624–652.

Braver, T. S., Barch, D., Gray, J. R., Molfese, D. L., & Snyder, A. Z. (2001). Anterior cingulate cortex and response conflict: Effects of frequency, inhibition, and errors. *Cerebral Cortex, 11,* 825–836.

Brown, J. W., & Braver, T. S. (2005). Learned predictions of error likelihood in the anterior cingulate cortex. *Science, 307,* 1118–1121.

Bush, G., Whalen, P. J., Rosen, B. R., Jenike, M. A., McInerney, S. C., & Rauch, S. L. (1998). The Counting Stroop: An interference task specialized for functional neuroimaging: Validation study with functional MRI. *Human Brain Mapping, 6,* 270–282.

Carlson, T., Grol, M. J., & Verstraten, F. A. (2006). Dynamics of visual recognition revealed by fMRI. *Neuroimage, 32,* 892–905.

Carter, C. S., Braver, T. S., Barch, D. M., Botvinick, M. M., Noll, D., & Cohen, J. D. (1998). Anterior cingulate cortex, error detection, and the online monitoring of performance. *Science, 280,* 747–749.

Cohen, J. D., MacWhinney, B., Flatt, M., & Provost, J. (1993). PsyScope: A new graphic interactive environment for designing psychology experiments. *Behavioral Research Methods, Instruments, and Computers, 25,* 257–271.

Coles, M. G., Scheffers, M. K., & Holroyd, C. B. (2001). Why is there an ERN/Ne on correct trials? Response representations, stimulus-related components, and the theory of error-processing. *Biological Psychology, 56,* 173–189.

Cook, E. P., & Maunsell, J. H. (2002). Dynamics of neuronal responses in macaque MT and VIP during motion detection. *Nature Neuroscience, 5,* 985–994.

Corbetta, M., Miezin, F., Dobmeyer, S., Shulman, G., & Petersen, S. (1991). Selective and divided attention during visual discriminations of shape, color, and speed: Functional anatomy by positron emission tomography. *Journal of Neuroscience, 11,* 2383–2402.

Debener, S., Ullsperger, M., Siegel, M., Fiehler, K., von Cramon, D. Y., & Engel, A. K. (2005). Trial-by-trial coupling of concurrent electroencephalogram and functional magnetic resonance imaging identifies the dynamics of performance monitoring. *Journal of Neuroscience, 25,* 11730–11737.

Dehaene, S., Posner, M., & Tucker, D. (1994). Localization of a neural system for error detection and compensation. *Psychological Science, 5,* 303–305.

D'Esposito, M., Detre, J. A., Alsop, D. C., Shin, R. K., Atlas, S., & Grossman, M. (1995). The neural basis of the central executive system of working memory. *Nature, 378,* 279–281.

Dosenbach, N., Visscher, K., Palmer, E., Miezin, F., Wenger, K., Kang, H., et al. (2006). A core system for the implementation of task sets. *Neuron, 50,* 799–812.

Falkenstein, M., Hohnsbein, J., Hoormann, J., & Blanke, L. (1991). Effects of crossmodal divided attention on late ERP

components: II. Error processing in choice reaction tasks. *Electroencephalography and Clinical Neurophysiology, 78,* 447–455.

Falkenstein, M., Hoormann, J., Christ, S., & Hohnsbein, J. (2000). ERP components on reaction errors and their functional significance: A tutorial. *Biological Psychology, 51,* 87–107.

Fellows, L. K. (2004). The cognitive neuroscience of human decision making: A review and conceptual framework. *Behavioral & Cognitive Neuroscience Reviews, 3,* 159–172.

Fleck, M. S., Daselaar, S. M., Dobbins, I. G., & Cabeza, R. (2006). Role of prefrontal and anterior cingulate regions in decision-making processes shared by memory and nonmemory tasks. *Cerebral Cortex, 16,* 1623–1630.

Fox, M. D., Snyder, A. Z., Barch, D. M., Gusnard, D. A., & Raichle, M. E. (2005). Transient BOLD responses at block transitions. *Neuroimage, 28,* 956–966.

Friston, K., Jezzard, P., & Turner, R. (1994). Analysis of functional MRI time-series. *Human Brain Mapping, 1,* 153–171.

Frith, C. D., & Dolan, R. J. (1997). Brain mechanisms associated with top–down processes in perception. *Philosophical Transactions of the Royal Society of London, Series B, Biological Sciences, 352,* 1221–1230.

Fuster, J. M. (1989). *Prefrontal cortex. Anatomy, physiology, and neuropsychology of the frontal lobe*. New York: Raven Press.

Gazzaley, A., Cooney, J. W., McEvoy, K., Knight, R. T., & D'Esposito, M. (2005). Top–down enhancement and suppression of the magnitude and speed of neural activity. *Journal of Cognitive Neuroscience, 17,* 507–517.

Gold, J., & Shadlen, M. (2007). The neural basis of decision making. *Annual Review of Neuroscience, 30,* 535–574.

Gold, J. I., & Shadlen, M. N. (2000). Representation of a perceptual decision in developing oculomotor commands. *Nature, 404,* 390–394.

Grinband, J., Hirsch, J., & Ferrera, V. (2006). A neural representation of categorization uncertainty in the human brain. *Neuron, 49,* 757–763.

Hampton, A. N., & O'Doherty, J. P. (2007). Decoding the neural substrates of reward-related decision making with functional MRI. *Proceedings of the National Academy of Sciences, U.S.A., 104,* 1377–1382.

Hanes, D. P., & Schall, J. D. (1996). Neural control of voluntary movement initiation. *Science, 274,* 427–430.

Holroyd, C. B., & Coles, M. G. H. (2002). The neural basis of human error processing: Reinforcement learning, dopamine, and the error-related negativity. *Psychological Review, 109,* 679–709.

James, T., Humphrey, G., Gati, J., Menon, R., & Goodale, M. (2000). The effects of visual object priming on brain activation before and after recognition. *Current Biology, 10,* 1017–1024.

Johnson, J. S., & Olshausen, B. A. (2005). The recognition of partially visible natural objects in the presence and absence of their occluders. *Vision Research, 45,* 3262–3276.

Kennerley, S. W., Walton, M. E., Behrens, T. E., Buckley, M. J., & Rushworth, M. F. (2006). Optimal decision making and the anterior cingulate cortex. *Nature Neuroscience, 9,* 940–947.

Kim, J.-N., & Shadlen, M. N. (1999). Neural correlates of a decision in the dorsolateral prefrontal cortex of the macaque. *Nature Neuroscience, 2,* 176–185.

Lancaster, J. L., Glass, T. G., Lankipalli, B. R., Downs, H., Mayberg, H., & Fox, P. T. (1995). A modality-independent approach to spatial normalization of tomographic images of the human brain. *Human Brain Mapping, 3,* 209–223.

Link, S., & Heath, R. (1975). A sequential theory of psychological discriminations. *Psychometrika, 40,* 77–105.

Lipshitz, R., Klein, G., Orasanu, J., & Salas, E. (2001). Taking stock of naturalistic decision making. *Journal of Behavioral Decision Making, 14,* 331–352.

Logan, G. (2002). An instance theory of attention and memory. *Psychological Review, 109,* 376–400.

Logothetis, N. K., & Sheinberg, D. L. (1996). Visual object recognition. *Annual Review of Neuroscience, 19,* 577–621.

Menon, V., Adleman, N. E., White, C. D., Glover, G. H., & Reiss, A. L. (2001). Error-related brain activation during a Go/NoGo response inhibition task. *Human Brain Mapping, 12,* 131–143.

Michelon, P., Snyder, A. Z., Buckner, R. L., McAvoy, M., & Zacks, J. M. (2003). Neural correlates of incongruous visual information. An event-related fMRI study. *Neuroimage, 19,* 1612–1626.

Miezin, F., Maccotta, L., Ollinger, J., Petersen, S., & Buckner, R. (2000). Characterizing the hemodynamic response: Effects of presentation rate, sampling procedure, and the possibility of ordering brain activity based on relative timing. *Neuroimage, 11,* 735–759.

Miller, E. K., & Cohen, J. D. (2001). An integrative theory of prefrontal cortex function. *Annual Review of Neuroscience, 24,* 167–202.

Ojemann, J. G., Akbudak, E., Snyder, A. Z., McKinstry, R. C., Raichle, M. E., & Conturo, T. E. (1997). Anatomic localization and quantitative analysis of gradient refocused echo-planar fMRI susceptibility artifacts. *Neuroimage, 6,* 156–167.

Ollinger, J. M., Corbetta, M., & Shulman, G. L. (2001). Separating processes within a trial in event-related functional MRI: II. Analysis. *Neuroimage, 13,* 218–229.

Ollinger, J. M., Shulman, G. L., & Corbetta, M. (2001). Separating processes within a trial in event-related functional MRI: I. The method. *Neuroimage, 13,* 210–217.

Parker, A., & Newsome, W. (1998). Sense and the single neuron: Probing the physiology of perception. *Annual Review of Neuroscience, 21,* 227–277.

Picard, N., & Strick, P. L. (1996). Motor areas of the medial wall: A review of their location and functional activation. *Cerebral Cortex, 6,* 342–353.

Platt, M. L., & Glimcher, P. W. (1999). Neural correlates of decision variables in parietal cortex. *Nature, 400,* 233–238.

Ploran, E. J., Nelson, S. M., Velanova, K., Donaldson, D. I., Petersen, S. E., & Wheeler, M. E. (2007). Evidence accumulation and the moment of recognition: Dissociating perceptual recognition processes using fMRI. *Journal of Neuroscience, 27,* 11912–11924.

Posner, M., & Rothbart, M. (2007). Research on attention networks as a model for the integration of psychological science. *Annual Review of Psychology, 58,* 1–23.

Posner, M. I., & Petersen, S. E. (1990). The attention system of the human brain. *Annual Review of Neuroscience, 13,* 25–42.

Posner, M. I., Petersen, S. E., Fox, P. T., & Raichle, M. E. (1988). Localization of cognitive operations in the human brain. *Science, 240,* 1627–1631.

Ratcliff, R. (1978). A theory of memory retrieval. *Psychological Review, 85,* 59–108.

Ratcliff, R., Cherian, A., & Segraves, M. (2003). A comparison of macaque behavior and superior colliculus neuronal activity to predictions from models of two-choice decisions. *Journal of Neurophysiology, 90,* 1392–1407.

Ratcliff, R., Hasegawa, Y. T., Hasegawa, R. P., Smith, P. L., & Segraves, M. A. (2007). Dual diffusion model for single-cell recording data from the superior colliculus in a brightness-discrimination task. *Journal of Neurophysiology, 97,* 1756–1774.

Rogers, R. D., Owen, A. M., Middleton, H. C., Williams, E. J., Pickard, J. D., Sahakian, B. J., et al. (1999). Choosing between small, likely rewards and large, unlikely rewards activates inferior and orbital prefrontal cortex. *Journal of Neuroscience, 19,* 9029–9038.

Roitman, J. D., & Shadlen, M. N. (2002). Response of neurons in the lateral intraparietal area during a combined visual discrimination reaction time task. *Journal of Neuroscience, 22,* 9475–9489.

Romo, R., & Salinas, E. (2003). Flutter discrimination: Neural codes, perception, memory and decision making. *Nature Reviews Neuroscience, 4,* 203–218.

Rossion, B., & Pourtois, G. (2004). Revisiting Snodgrass and Vanderwart's object pictorial set: The role of surface detail in basic-level object recognition. *Perception, 33,* 217–236.

Sanfey, A. G., Rilling, J. K., Aronson, J. A., Nystrom, L. E., & Cohen, J. D. (2003). The neural basis of economic decision-making in the Ultimatum Game. *Science, 300,* 1755–1758.

Scheffers, M. K., & Coles, M. G. H. (2000). Performance monitoring in a confusing world: Error-related brain activity, judgments of response accuracy, and types of errors. *Journal of Experimental Psychology: Human Perception and Performance, 26,* 141–151.

Shadlen, M. N., & Newsome, W. T. (2001). Neural basis of a perceptual decision in the parietal cortex (area LIP) of the rhesus monkey. *Journal of Neurophysiology, 86,* 1916–1936.

Smith, P. L., & Vickers, D. (1988). The accumulator model of two-choice discrimination. *Journal of Mathematical Psychology, 32,* 135–168.

Snyder, A. Z. (1996). Difference image versus ratio image error function forms in PET–PET realignment. In D. Bailey & T. Jones (Eds.), *Quantification of brain function using PET.* San Diego: Academic Press.

Talairach, J., & Tournoux, P. (1988). *Co-planar stereotaxic atlas of the human brain.* New York: Thieme.

Thielscher, A., & Pessoa, L. (2007). Neural correlates of perceptual choice and decision making during fear–disgust discrimination. *Journal of Neuroscience, 27,* 2908–2917.

Usher, M., & McClelland, J. L. (2001). The time course of perceptual choice: The leaky, competing accumulator model. *Psychological Review, 108,* 550–592.

Vickers, D. (1970). Evidence for an accumulator of psychophysical discrimination. *Ergonomics, 13,* 37–58.

Vogt, B. A., Finch, D. M., & Olson, C. R. (1992). Functional heterogeneity in cingulate cortex: The anterior executive and posterior evaluative regions. *Cerebral Cortex, 2,* 435–443.

Winer, B., Brown, D., & Michels, K. (1991). *Statistical principles in experimental design.* New York: McGraw-Hill.

Yeung, N., Cohen, J. D., & Botvinick, M. M. (2004). The neural basis of error detection: Conflict monitoring and the error-related negativity. *Psychological Review, 111,* 931–959.